Distribution Agreement

In presenting this thesis as a partial fulfillment of the requirements for a degree from Emory University, I hereby grant to Emory University and its agents the non-exclusive license to archive, make accessible, and display my thesis in whole or in part in all forms of media, now or hereafter now, including display on the World Wide Web. I understand that I may select some access restrictions as part of the online submission of this thesis. I retain all ownership rights to the copyright of the thesis. I also retain the right to use in future works (such as articles or books) all or part of this thesis.

Weiyi Tian March 31, 2022

Localization of mRNAs to Centrosomes Requires the Pericentriolar Material Scaffold

By

Weiyi Tian

Dr. Dorothy A. Lerit, Ph.D.
Adviser

Biology

Dr. Dorothy A. Lerit, Ph.D.

Adviser

Dr. Frank McDonald, Ph.D.

Committee Member

Dr. Leila Rieder, Ph.D.

Committee Member

2023

Localization of mRNAs to Centrosomes Requires the Pericentriolar Material Scaffold

By

Weiyi Tian

Dr. Dorothy A. Lerit, Ph.D.

Advisor

An abstract of
a thesis submitted to the Faculty of Emory College of Arts and Sciences
of Emory University in partial fulfillment
of the requirements of the degree of
Bachelor of Science with Honors

Biology

2023

Abstract

Localization of mRNAs to Centrosomes Requires the Pericentriolar Material Scaffold
By Weiyi Tian

The pericentriolar material (PCM) is a proteinaceous matrix surrounding the centrioles that promotes centrosome microtubule-nucleating activity. We and others previously showed the pericentriolar components Centrosomin (Cnn) and Pericentrin-like protein (PLP) functionally cooperate to organize a PCM scaffold required for centrosome structure and microtubule organization. We recently showed that several centrosomal mRNAs are localized to the centrosome and contribute to centrosome function under the regulation of RNA-binding proteins. However, whether the PCM is required to recruit or anchor mRNA to the centrosome remains incompletely understood. We hypothesize that PCM functions as a scaffold to anchor centrosomal mRNAs at centrosomes. To test our hypothesis, we used a classic *cnn* allele to disrupt PCM organization and investigated consequences to the localization of *centrocortin* (*cen*) and *plp* mRNAs. We used super-resolution imaging and quantitative single-molecule fluorescence in situ hybridization (smFISH) to visualize and quantify mRNA enrichments at centrosomes in syncytial *Drosophila* embryos. We also adapted our customizable Subcellular Distribution computational pipeline and compared mRNA distributions as quantified from either the centroid or surface of centrioles to permit quantification using a variety of centrosome markers. Upon disrupting PCM organization, our data indicate that the enrichment of *cen* mRNAs at centrosomes and the distribution of *cen* mRNA within granules are significantly decreased. Similarly, we observed a significant decrease in *plp* mRNA localization to centrosomes in *cnn* mutants. These data demonstrate that the PCM scaffold is needed for *cen* and *plp* mRNA localization to centrosomes and for packaging *cen* mRNA into higher-order RNA granules. Our work helps elucidate mechanisms of mRNA localization to centrosomes.

Localization of mRNAs to Centrosomes Requires the Pericentriolar Material Scaffold

By

Weiyi Tian

Dr. Dorothy A. Lerit, Ph.D.
Advisor

A thesis submitted to the Faculty of Emory College of Arts and Sciences
of Emory University in partial fulfillment
of the requirements of the degree of
Bachelor of Science with Honors

Biology

2023

Acknowledgements

I would like to express my appreciation to my thesis advisor, Dr. Dorothy A. Lerit, and my research mentor, Dr. Junnan Fang, for their support since the beginning of my honors research work. I would also like to thank the members of the Lerit lab for providing me with a pathway and help to perform this work. The completion of this thesis would not have been possible without the support I have received from the Lerit lab. I appreciate Dr. Jordan Beach and Melissa Quintanilla from Loyola University Chicago for their collaboration on super-resolution imaging using their ZEISS Airyscan Microscope.

Additionally, I acknowledge Dr. Frank McDonald and Dr. Leila Rieder for being on my honors thesis committee and providing helpful suggestions for improvements.

Lastly, I want to thank my family and dearest friends, who have been my firmest mental support during this journey.

Table of Contents

List of Figures

List of Tables

Chapter 1

Localization of mRNAs to Centrosomes Requires the PCM Scaffold

1.1 Introduction

The centrosome is the microtubule-organizing center of most animal cells and is composed of a pair of centrioles surrounded by a matrix of proteins called the pericentriolar material (PCM; Conduit et al., 2015). The PCM oscillates in concert with different cell cycle stages, referred as the PCM dynamic, to confer the functional changes of centrosome activity. In prototypical cells, PCM levels increase in preparation for mitosis, but decrease at mitotic exit (Figure 1; Khodjakov and Rieder, 1999). Upon mitotic entry, PCM levels increase in a process called centrosome maturation by recruiting more proteins to help organize the bipolar mitotic spindle (Palazzo et al., 2000). Following mitotic exit, centrosomes shed PCM. PCM protein levels decrease to allow the centrosome to facilitate cell migration, intracellular trafficking, and ciliogenesis (Magescas et al., 2019; Mittasch et al., 2020). The recruitment and organization of PCM is facilitated through the presence of a PCM scaffold, mainly composed of Centrosomin (Cnn) and Pericentrin-like protein (PLP; Figure 1), or their mammalian orthologs, CDK5RAP2/CEP215 and Pericentrin (PCNT; Lerit et al., 2015). Within *Drosophila* embryos, the PCM scaffold expands during interphase as PLP localizes to the tips of Cnn flares and forms satellites (Lerit et al., 2015). PCM dynamics are key to centrosome regulation, and their deregulation leads to microcephaly, ciliopathy, cancer, and other diseases (Conduit et al., 2015; Nigg and Raff, 2009).

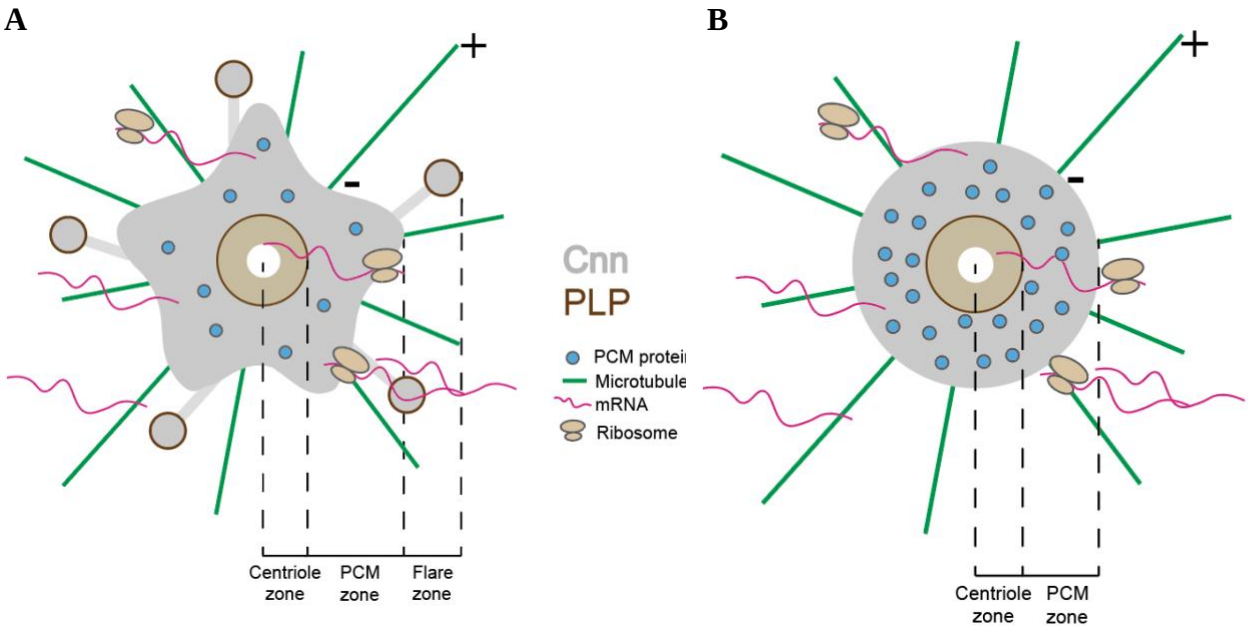

Figure 1. Diagrams of the PCM scaffold structure and centrosome zones in (A) interphase and (B) mitosis. Cnn and PLP cooperate to form the PCM scaffold. PCM levels increase during mitosis and decrease during interphase.

Many findings suggest that the PCM dynamic is regulated by posttranscriptional paradigms: mRNA localization and translational control. Early *Drosophila* embryos are largely transcriptionally quiescent and, therefore, are subject to posttranscriptional controls (Vastenhouw et al., 2019). Their centrosomes rely on a maternal supply of mRNA and proteins to coordinate nuclear migration and divisions essential for embryogenesis, which rapidly proceeds through 14 abridged nuclear cycles (NCs) that lack gap phases (Foe and Alberts, 1983). Through a genome-wide RNA localization high-throughput screen in early *Drosophila* embryos, a subset of mRNAs was discovered at centrosomes (Lécuyer et al., 2007). Consistent with this screen, recent work from our lab showed that *centrocortin* (*cen*) and *plp* mRNAs undergo cell-cycle dependent localization to centrosomes using quantitative single-molecule fluorescence in situ hybridization (smFISH; Ryder et al., 2020). Moreover, the localization of mRNAs to centrosomes is observed

in diverse cell types and various species, including neurons, fibroblasts, and embryos of Xenopus, zebrafish, and mollusk (Buxbaum et al., 2015). This conserved enrichment of mRNAs at centrosomes hints that centrosomes functions may be regulated by localized mRNAs (Vastenhouw et al., 2019).

Notably, many of the mRNAs that are localized to the centrosome encode for centrosome regulatory proteins, including cyclin B (*cyc B*) and *plp,* which raises the possibility that RNA localization and local translation are coupled (Dalby and Glover, 1992; Martinez-Campos et al., 2004; Raff et al., 1990). Early studies revealed the presence of ribosomes, the sites of protein synthesis, around centrioles and basal bodies via electron microscopy (Sorokin 1962). Consistent with the idea of local translation, recent works implicated a co-translational transport mechanism for several centrosome-localized mRNAs. Using dual mRNA and protein labeling, several centrosomal protein-coding mRNAs are found to co-localize with their proteins to centrosomes (Chouaib et al., 2020; Safieddine et al., 2021). In addition, puromycin sensitivity assays implicate translating polysomes reside at centrosomes (Sepulveda et al., 2018).

Given the numerous implications of mRNA localization to regulate centrosome functions, we are interested in elucidating its functional consequences and mechanisms. We recently found that deregulation of *cen* mRNA localization to the centrosome in the absence of its regulatory protein, fragile-X mental retardation protein (FMRP), causes mitotic spindle defects (Ryder et al., 2020). Likewise, ectopic *cen* mRNA localization prevented the localization of Cen protein to distal centrosomes and caused error-prone mitosis in *Drosophila* embryos (Ryder et al., 2020). These studies revealed local levels of *cen* mRNA influence embryonic nuclear divisions and genome stability. These results strongly support a model that centrosomal

cen mRNA localized at centrosomes are precisely tuned for centrosome activity. Nonetheless, the mechanism of *cen* mRNA localization to centrosomes remain largely unexplored.

Also localizing to centrosomes is *plp* mRNA, which encodes for PLP, the ortholog of human *PCNT* (Martinez-Campos et al., 2004). Like *plp* mRNA, *pcnt* mRNA is found to be enriched at centrosomes in both mammalian cells and zebrafish embryos (Sepulveda et al., 2018). Loss of *plp* in *Drosophila* results in embryonic lethality, and deregulation of human *PCNT* is associated with severe genetic disorders, such as Down syndrome and microcephalic osteodysplastic primordial dwarfism type II (MOPD II; Rauch et al., 2008). Recent data from our lab indicates that the cytoplasmic polyadenylation element binding (CPEB) protein ortholog, Oo18 RNA-binding protein (Orb), is dispensable for *plp* mRNA localization to centrosomes. Rather, Orb binds to the 3′-untranslated region (UTR) of *plp* mRNA to promote polyadenylation and PLP protein translation. In the absence of Orb, PLP protein localization to centrosomes is significantly reduced, resulting in compromised PCM scaffolding function that leads to genomic instability (Fang and Lerit, 2022). However, little is known about how *plp* mRNA localizes to the centrosome.

Here, we show that the PCM functions as a scaffold to anchor centrosomal mRNAs at centrosomes. To test whether PCM scaffold is required for mRNAs localization to centrosomes, we disassembled the PCM organization around the centrioles using a point mutation, cnn^{B4}, in *Drosophila* and investigated its consequences on mRNA enrichments at centrosomes. We visualized changes to mRNA distributions using smFISH coupled with spinning disk microscopy and super-resolution imaging. To quantify RNA localization patterns in control versus mutant samples, we employed a custom Python-based analysis package, Subcellular Distribution, developed by our lab to measure object-to-object distances and analyze the percentage of

mRNAs at the centrosomes. These assays confirmed a significant decrease in centrosome-localized mRNA upon PCM disruption. To determine whether the observed reduction in RNA localization is caused by reduced steady-state mRNA levels, we performed RT-qPCR from WT versus *cnnB4* embryo extracts. We found no significant change in *plp* mRNA levels but note a decrease in *cen* mRNA levels in the mutants. These data suggest that the PCM functions as a scaffold to anchor centrosomal mRNAs to support their localization to centrosomes. Lastly, to get a more comprehensive view of how the PCM scaffold impacts mRNA localization, we are using an independent method to disrupt PCM organization through the generation of null *plp* germline clones to study how *cen* mRNA localization changes as the PCM structure is disrupted due to absence of PLP. Our completed and ongoing work aims to uncover the basis for RNA localization to centrosomes and to investigate how local RNAs contribute to centrosome function.

1.2 Results

1.2.1 *cen* mRNA Localization to Centrosomes and Granule Formation Decreases upon PCM Disruption

Cen protein binds to Cnn protein directly, and they function in the PCM to help coordinate cleavage furrow assembly in *Drosophila* embryos (Kao and Megraw, 2009). Prior studies from our lab showed that *cen* mRNA enrichment at centrosomes is significantly higher than *gapdh* (>50% higher in NC 13 embryos), a non-localizing mRNA that disperses throughout the cytoplasm (Ryder et al., 2020). *cen* mRNA localization to centrosomes is cell cycle stage-dependent, with around 60% *cen* localized during interphase and only about 25% during

metaphase in NC 13 embryos (Ryder et al., 2020). As more *cen* overlaps with interphase centrosomes, we choose to investigate the RNA localizing mechanism in interphase *Drosophila* embryos in more detail. The localization of *cen* mRNA to centrosomes has a unique feature that it localizes mostly as single molecules until NC 13, when it assembled into micrometer-scale granules (Ryder et al., 2020). Thus, we selected interphase NC 13 embryos to quantify RNA localization and inclusion within granules, which is computationally defined as a structure containing four or more single mRNA molecules (Ryder and Lerit, 2020).

To test whether an intact PCM structure is required for mRNA localization to centrosomes, we used the cnn^{B4} mutation to disrupt the PCM organization and studied its consequences to mRNA enrichments at centrosomes. cnn^{B4} is a missense mutation of a highly conserved Arginine residue, leading to an R1141H substitution in the broadly conserved Cnn motif 2 of the *cnn* gene. The cnn^{B4} mutation was previously shown to disassemble the PCM around centrioles while retaining the microtubule organizing activity (Figure 2; Kao and Megraw, 2009). To visualize the enrichment of *cen* mRNA at centrosomes, we used smFISH to detect single RNA molecules and coupled it with immunofluorescence of centrosomal proteins, Asterless (Asl) and Cnn (Femino et al., 1998). We chose Asl as the centrosome marker because it resides in the centriole zone and, therefore, is unaffected by PCM disruption. Cnn was labeled to contrast the intact versus disassembled PCM in WT and cnn^{B4} mutants. Because the *Drosophila* embryo centrosome is about 1 μm in diameter, we examined PCM organization relative to smFISH signals using super-resolution microscopy. Using Zeiss Airyscan super-resolution microscopy, we found that *cen* is enriched at centrosomes and forms granules in interphase NC 13 *Drosophila* embryos with intact PCM structures, consistent with our prior work (Figure 3A). In contrast, we found less *cen* enrichment at centrosomes and less granule

formation associated with the disrupted PCM organization in *cnn*^{B4} mutants (Figure 3B). These data suggest that the PCM scaffold is required for *cen* mRNA to form granules and localize to centrosomes.

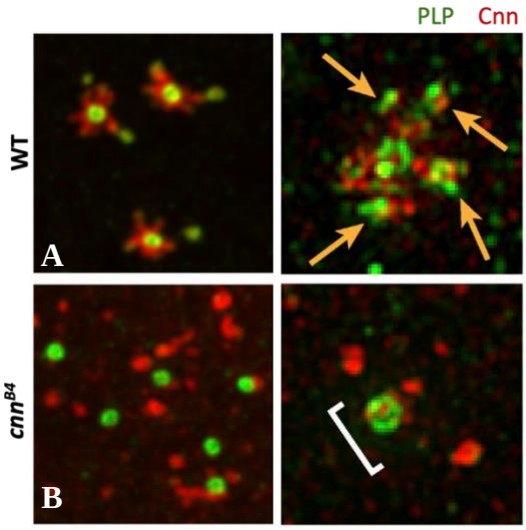

Figure 2. *cnn*^{B4} disrupts the PCM organization. (Adapted from Lerit et al., 2015) Confocal microscopy images (A) and SIM images (B) show *cnn*^{B4} mutants do not properly assemble PCM around the centriole (bracket)[3].

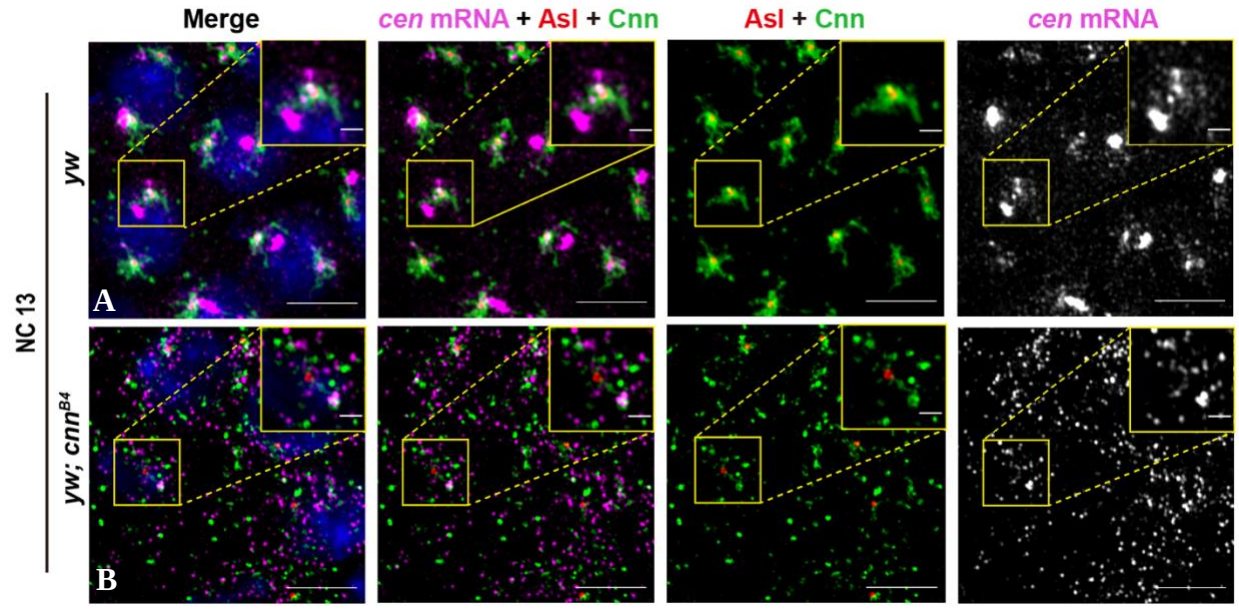

Figure 3. *cen* mRNA localization to centrosomes and granule formation decreases upon PCM disruption. Super-resolution images showing smFISH of *cen* mRNA (magenta) at centrosomes labelled by Asl (red) and Cnn (green) in NC 13 **(A)** WT and **(B)** cnn^{B4} mutant embryos. Scale bars: 5 μm; 1 μm (insets).

1.2.2 Quantification of the *cen* mRNA Enrichment at Centrosomes in WT vs. cnn^{B4} Mutants

To measure changes to *cen* mRNA localization to centrosomes, we examined NC 11 and 13 embryos by spinning disk confocal microscopy then quantified RNA distributions using a Subcellular Distribution pipeline developed by our lab. To obtain a higher signal-to-noise ratio, necessary for image segmentation before quantification, we combined smFISH with endogenous expression of Asl-YFP to label centrosomes. Consistent with super-resolution imaging, confocal images show less *cen* mRNA resided in granules and enriched at centrosomes upon PCM disruption in NC 11 and 13 embryos (Figure 4A-D).

Next, we used the pipeline to measure the distances between individual RNA objects and the centriole surface of their closest centrosome. Our prior work indicates interphase *Drosophila* embryonic centrioles occupy a much smaller volume (~200 nm diameter, or approximately $4.19x10^6$ nm^3 volume) as compared to the PCM (~1500 nm diameter, or $1.77x10^9$ nm^3; Lerit et al., 2015) . Given the significantly smaller volume of centrioles compared to centrosomes, we calculated the percentage of mRNAs within 1 μm of the centriole surface as overlapping with centrosomes. Our quantification indicates a ~30% decrease in *cen* mRNA and granule enrichment at centrosomes upon PCM disruption in interphase NC 11 embryos (Figure 4E&F). In NC 13 mutant embryos, quantification reveals that ~40% less *cen* localizes and ~45% less *cen* forms granules in cnn^{B4} mutants as compared to controls (Figure 4G&H). These data

demonstrate that an organized PCM is required for *cen* mRNA localization to centrosomes and organization into higher-order granules.

It is technically feasible that the RNA signals overlapping with centrosomes may reflect a spurious overlap due to chance. To demonstrate the RNA overlapping with centrosomes represents bona fide localization, we rotated the RNA channel by 90° and then compared the percentage of RNA at centrosomes before and after rotation. Following channel rotation, the RNA enrichment showed a significant decrease in NC 11 and 13 embryos (Figure 4I&J). This image rotation process validates the specificity of *cen* mRNA enrichment at centrosomes, indicating that the PCM dissemblance significantly disrupted the *cen* mRNA localization to centrosomes.

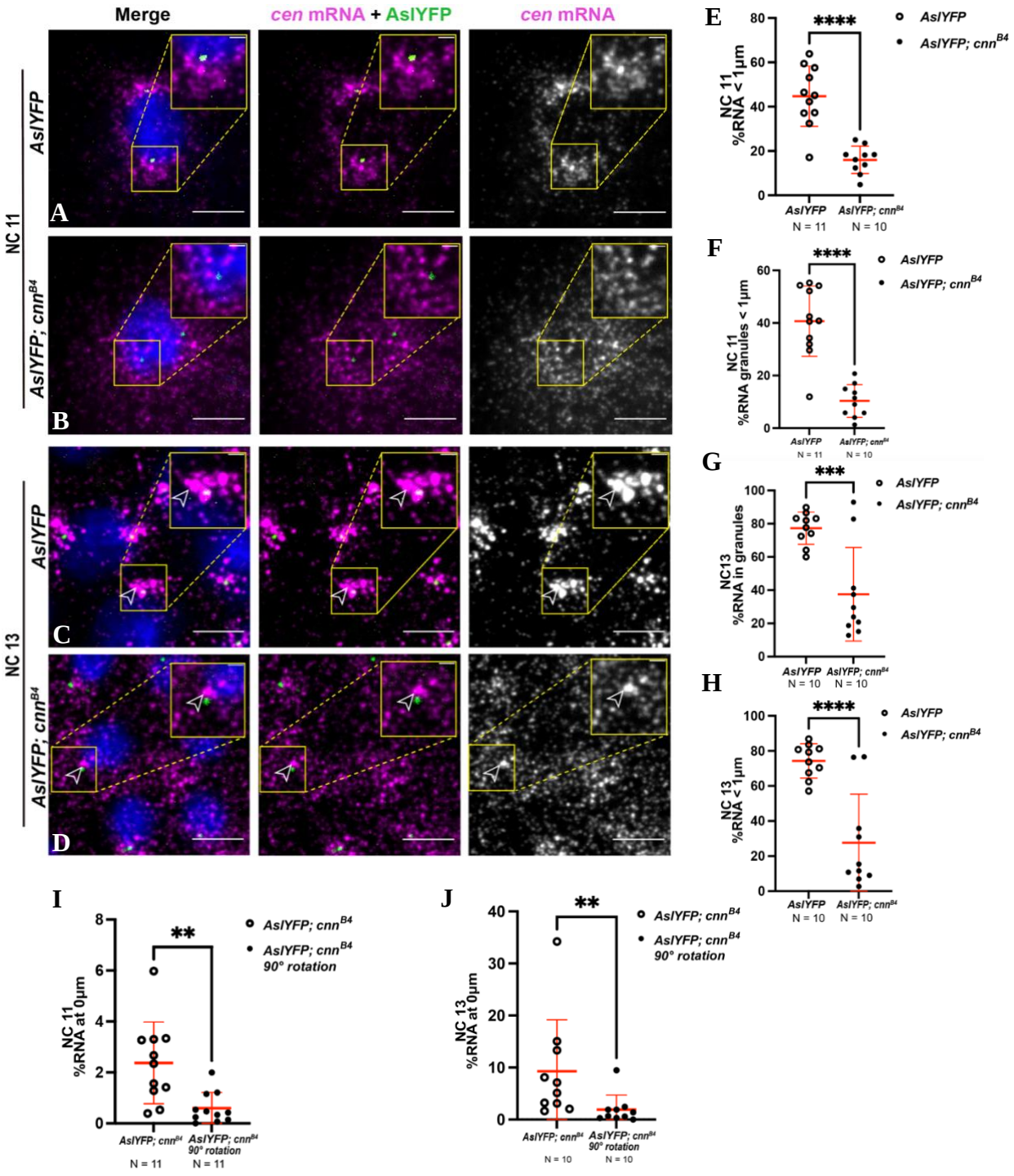

Figure 4. Quantification of reduced *cen* mRNA localization to centrosomes and granule formation upon PCM disruption. (A-D) Maximum-intensity projections of smFISH for *cen* mRNA (magenta) in interphase NC 11 and 13 embryos expressing Asl-YFP (green). Arrow indicates *cen* mRNA granules. **(E-H)** Quantification of the percentage of RNA and RNA

granules within 1 μm from the centriole zone surface, where each dot represents a single measurement from n = 11 interphase NC 11 WT, 10 interphase NC 11 mutant, and 10 NC 13 WT and mutant embryos, respectively. Mean ± SD are shown (red text). **, P < 0.01; ***, P < 0.001; ****, P < 0.0001 by unpaired *t*-test. **(I-J)** Quantification of percentage *cen* mRNA at centrosomes before and after 90° RNA channel rotation in interphase **(I)** NC 11 and **(J)** 13 mutant embryos. Scale bars: 5 μm; 1 μm (insets).

1.2.3 Localization of *plp* mRNA to Centrosomes Decreases upon PCM Disruption

Our data show an organized PCM supports *cen* mRNA localization. Next, we investigated whether *plp* mRNA localization to centrosomes is similarly affected upon PCM disruption. PLP, like *PCNT*, is a key protein component of the PCM scaffold supporting the PCM organization essential for centrosome functioning (Lerit et al., 2015; Lerit and Rusan, 2013).

Unlike *cen* mRNA, *plp* localizes to centrosomes as single molecules throughout the syncytial development of early *Drosophila* embryos (Ryder et al., 2020). Our prior work indicates the degree of *plp* enrichment at centrosomes is more modest than *cen*, and only ~10% higher than the control *gapdh* (Ryder et al., 2020). Super-resolution images of NC 13 embryos show that *plp* mRNA is enriched at centrosomes with an intact PCM scaffold in WT embryos. In contrast, *plp* mRNA enrichment is reduced at centrosomes with a disassembled PCM structure in cnn^{B4} mutant embryos (Figure 5). These data indicate that *plp* mRNA localization to centrosomes is also supported by an intact PCM scaffold, similar to *cen* mRNA.

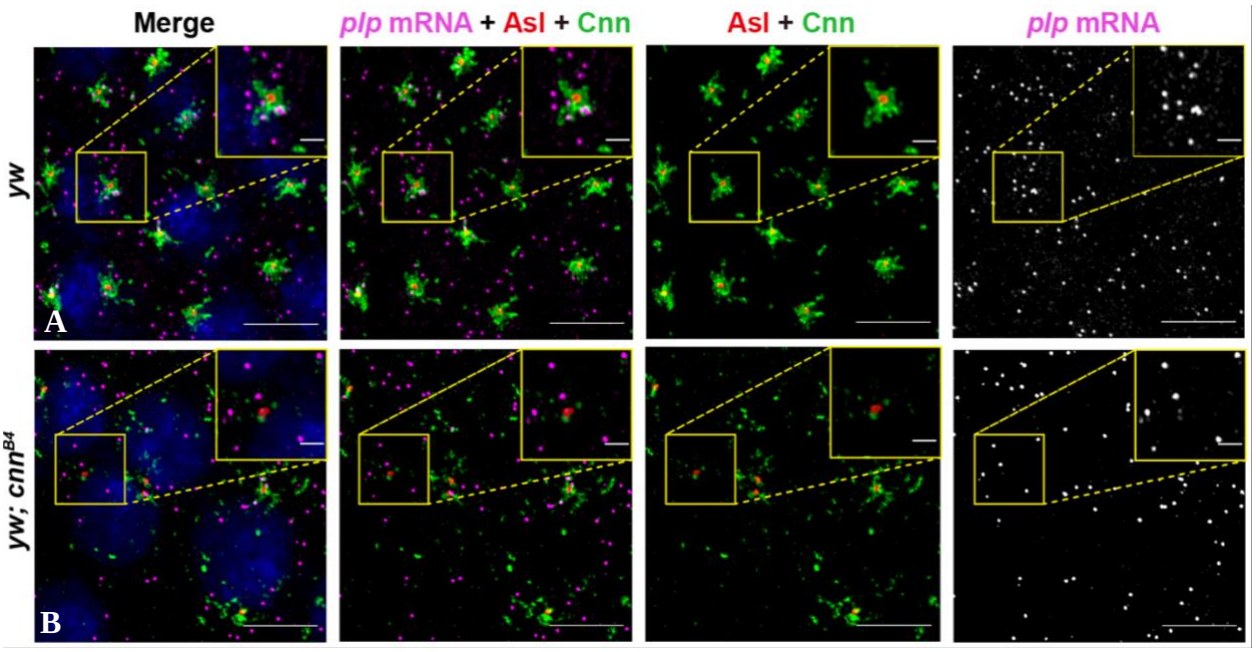

Figure 5. *plp* mRNA localization to centrosomes decreases upon PCM disruption. Super-resolution images showing smFISH of *plp* mRNA (magenta) at centrosomes labelled by Asl (red) and Cnn (green) in NC 13 **(A)** WT and **(B)** cnn^{B4} mutant embryos. Scale bars: 5 µm; 1 µm (insets).

To quantify the significance of this decrease, we again quantified confocal images of *plp* enrichment at centrosomes in WT vs. mutant NC 11 and 13 embryos (Figure 6A-D). Quantification confirmed a significant reduction in *plp* mRNA enrichment upon PCM disruption with approximately ~10% less *plp* mRNA localizing to centrosomes at either NC 11 or NC 13 (Figure 6E-F). These data indicate that *plp* mRNA localization to centrosomes also requires the PCM scaffold, suggesting a general need of this scaffold for mRNA localization.

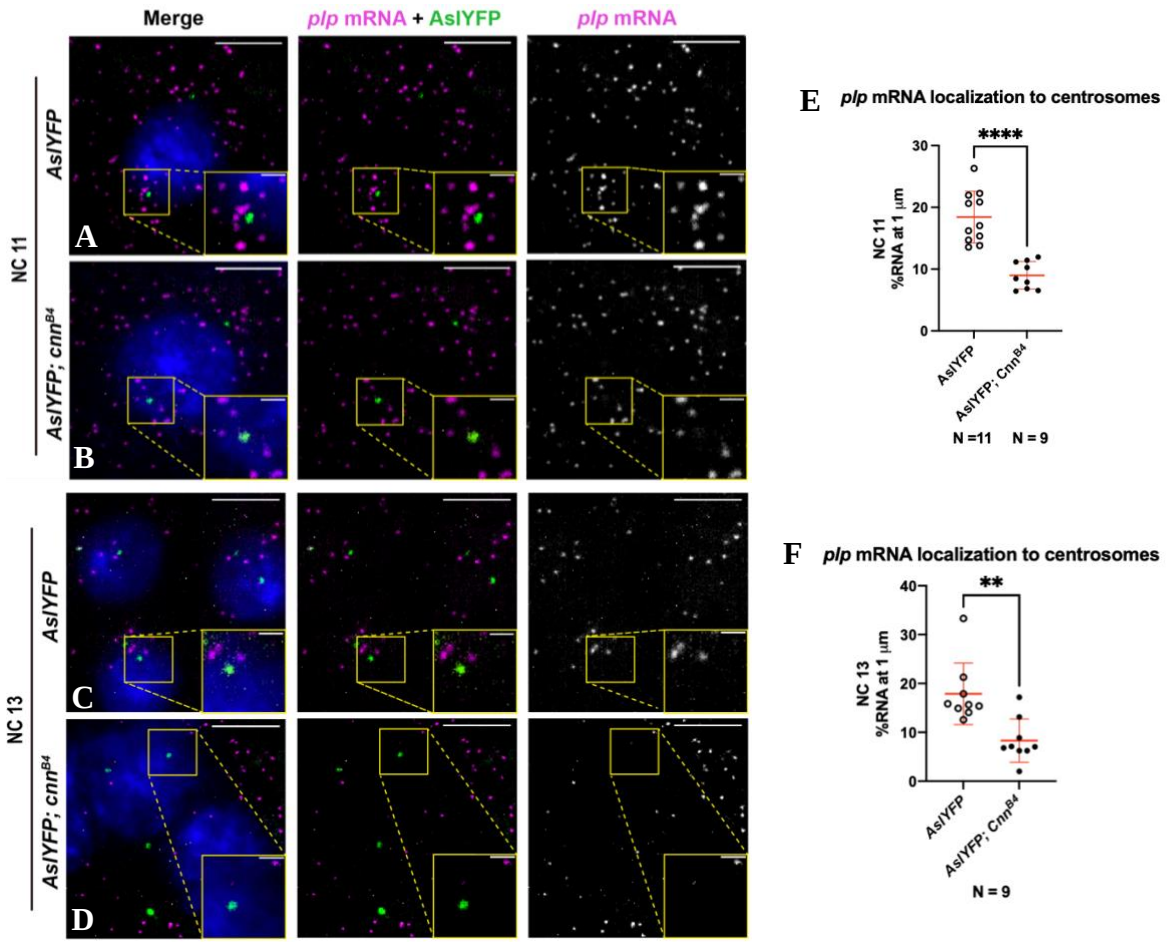

Figure 6. Quantification of reduced *plp* mRNA localization to centrosomes upon PCM disruption. (A-D) Maximum-intensity projections of smFISH for *plp* mRNA (magenta) in interphase NC 11 and NC 13 embryos expressing Asl-YFP (green). **(E-F)** Quantification of the percentage of RNA within 1 µm from the centriole zone surface, where each dot represents a single measurement from n = 11 interphase NC 11 WT, 9 interphase NC 11 mutant, and 9 NC 13 WT and mutant embryos, respectively. Mean ± SD are shown (red text). **, P < 0.01; ***, P < 0.001; ****, P < 0.0001 by unpaired *t*-test. Scale bars: 5 µm; 1 µm (insets).

1.2.4 Decrease in RNA localization is Not Caused by Whole-cell RNA Level Reduction

Our data suggest that an intact PCM is required for robust mRNA localization to centrosomes. However, it is formally possible the reduced levels of RNA we observe at cnn^{B4} centrosomes may be attributed to a decrease in RNA levels, thereby obfuscating quantification of localization. To assay steady-state RNA levels, we conducted qPCR to compare the RNA levels in 0-2 h

control versus *cnn*^{B4} embryos. There was no significant difference in *plp* mRNA levels in WT versus mutant embryos. In contrast, levels of *cen* mRNA are reduced by about 30% in *cnn*^{B4} mutant embryos relative to controls (Figure 7). These data suggest that impaired PCM integrity through the *cnn*^{B4} mutation does not compromise *plp* mRNA stability. In contrast, the reduced *cen* mRNA levels observed in *cnn*^{B4} mutants may contribute to impaired RNA localization to centrosomes. However, we do note approximately 40% less *cen* mRNA localizes to centrosomes in *cnn*^{B4} mutants, while RNA levels are only reduced by 30%, suggesting that decreased *cen* mRNA localization is not fully counted by the whole-cell RNA level reduction.

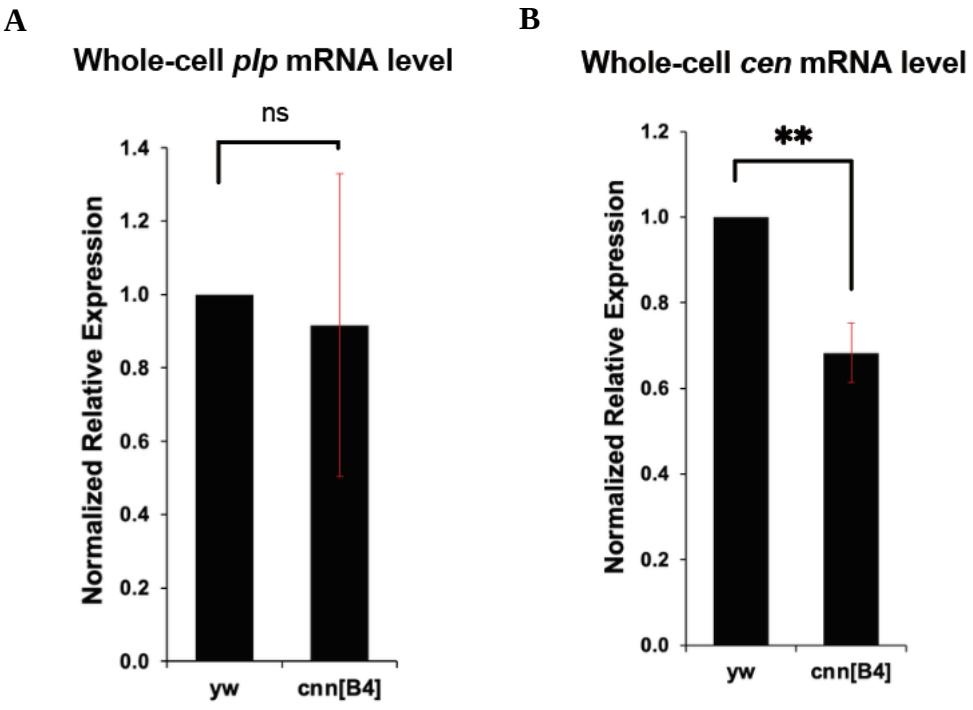

Figure 7. *plp* mRNA expression level shows no significance difference in *yw* vs *cnn*^{B4} mutant embryos, while *cen* mRNA expression level reduces in *cnn*^{B4} embryos. Relative levels of total **(A)** *plp* mRNA and **(B)** *cen* mRNA normalized to *RP49* mRNA were examined by RT-qPCR in 0-2h-old WT and *cnn*^{B4} mutant embryos from three replicates; $^{**}P<0.01$ by unpaired *t*-test. Measured in arbitrary units.

1.3 Discussion

As the major microtubule organizing centers in most mammalian cells, centrosomes are tightly regulated by the localization of a subset of mRNAs and their local translation to facilitate normal development. Our recent work reveals precisely tuned *cen* mRNA localization to centrosomes is needed to facilitate error-free mitosis and a requirement of regular PLP protein levels to support PCM scaffolding. Despite this biological importance, the mechanisms of these mRNAs localizing to centrosomes remained to be explored. To test how the mRNAs are anchored at centrosomes, we showed a reduction in *cen* and *plp* mRNA recruitment to centrosomes upon disruption of the PCM scaffold, which functions to support the centrosome structure. Moreover, we found the disassembled PCM structure impeded the assembly of *cen* mRNAs to form granules at centrosomes. These data suggest either the presence of a PCM scaffold is upstream of the mRNA localization to centrosomes or required for anchorage of localized mRNAs. Further, localization of *cen* mRNA to centrosomes may facilitate granule formation or stability. Although we found that *cen* mRNA localization reduction is associated with whole-cell RNA reduction, we need to be careful on concluding a causal inference. Localized mRNAs may be stabilized at centrosomes to avoid targeted degradation. Thus, we cannot be sure whether the whole-cell RNA reduction is a cause or result of reduced RNA localization. Further analysis needs to be done to test the significance of decreased *cen* mRNA localization to centrosomes in cnn^{B4} mutant.

cen mRNA enrichment at centrosomes in NC 11 embryos upon PCM disruption decreases from 45% to 16%, which is a 64% reduction change. Strikingly, NC 13 embryos show a decrease from 77.3% to 37.5%, which yields a 52% reduction change, lower than that in NC 11. This smaller decrease may suggest that the mRNA anchoring ability of the PCM scaffold is

subject to developmental stages of embryos or be a physical constraint owing to the correspondingly smaller volume of NC 13 pseudocells. In accordance with higher mRNA enrichment at centrosomes in later embryo development, PCM scaffolding ability may increase to recruit more mRNA. Thus, the strengthening of the anchoring ability may partly compensate for the RNA reduction upon PCM disruption. However, further studies are needed to investigate whether this elevated anchoring ability is achieved by stronger molecular interactions, increased local concentration of the scaffolding proteins, PLP and Cnn, or the recruitment of as-yet unidentified factors that facilitate mRNA anchorage, for example, RNA-binding proteins.

Our finding that the PCM scaffold is required for mRNA to localize to centrosomes, motivates examination of how RNA localization responds to other PCM disruptions. To test this question, we are generating *plp* null germline clones to study the consequences to RNA localization to centrosomes. The *plp* null mutation would completely deprive PLP in the PCM scaffold, causing a severe disruption of the PCM (Lerit et al., 2015). Percentage changes in *cen* mRNA enrichment at centrosomes will be compared to controls and cnn^{B4} mutants to more comprehensively examine if PCM organization is a general requirement for RNA localization. An alternative possibility is the reduction in RNA localization we observe is due to defined protein-protein interactions between Cnn and Cen or PLP, as previously described by our group and others (Kao and Megraw, 2009; Lerit et al., 2015). In this model, protein interactions may direct localization of the RNA, consistent with the favored co-translational transport model prevalent in the literature.

1.4 Materials and Experimental Procedures

Fly Stocks

The following *Drosophila* strains were used: y^1w^{1118} (1495; Bloomington *Drosophila* Stock Center) and *Asl-YFP*, which expresses Asterless (Asl) tagged with YFP under the control of the polyubiquitin promoter (Rebollo et al., 2007), were used as the WT control; and cnn^{B4} is a hypomorphic allele caused by an R1141H single amino acid mutation (Vaizel-Ohayon and Schejter, 1999), a gift from T. Megraw (Florida State University, Tallahassee, FL). Flies were maintained on cornmeal-based *Drosophila* medium (LabExpress, Bloomington formulation) at 25°C in a light- and temperature-controlled chamber.

Embryo Collection and Fixation

0.5-2.5 hour embryos were collected from fly cages on grape agar plates and dechorionated with bleach. Embryos were then rinsed with water and shaked for 30 s in a 1:1 solution of heptane/anhydrous methanol before devitellinization in methanol.

Detection of RNA by smFISH

All steps were performed with RNase-free solutions. Fixed embryos were rehydrated stepwise in 7:3, 1:1, and 3:7 solutions of Methanol/PBST (PBS plus 0.1% Tween-20) and then washed in PBST and prewarmed wash buffer (WB; 10% formamide and 2X SSC) freshly supplemented with 0.1% Tween-20 and 2 µg/ml nuclease-free BSA [0332-25G; VWR]) at RT with nutation. Embryos were then incubated with 100 µl of hybridization buffer (HB; 100 mg/ml dextran sulfate and 10% formamide in 2X SSC) freshly supplemented with 0.1% Tween-20, 2µg/ml

nuclease-free BSA, and 10 mM ribonucleoside vanadyl complex (RVC; S1402S; New England Biolabs) for 10–20 min in a 37°C water bath. Stellaris *cen* and *plp* smFISH probes conjugated to Quasar 570 dye (LGC Biosearch Technologies) were diluted 1:50 in 25 µl HB with supplements and incubated in a 37°C water bath overnight. Embryos were washed in WB with supplements, stained with DAPI (1:1000 diluted in PBST) for 1 h, washed with PBST at RT with mutation, and mounted with Vectashield mounting medium (H-1000; Vector Laboratories). Slides were sealed with nail polish, stored at 4°C avoiding light, and imaged within 1 week.

Dual immunofluorescence and smFISH

This protocol is optimized based on that of Xu et al., 2015. After incubation in HB with supplements for 10–20 min in a 37°C water bath, embryos were incubated in 25 µl HB with supplements containing both diluted smFISH probes and primary antibodies, rabbit anti-Asl (1:4000) and guinea pig anti-Cnn (1:3000), overnight at 37°C. The following day, embryos were washed twice for 30 minutes each in WB with supplements, followed by two 15-min and two 30-min washes in WB at RT with nutation. Secondary antibodies (1:500), Alexa Fluor 488 and 647, and DAPI were diluted into WB to incubate the embryos for 2 h at RT with nutation. Embryos were then washed in PBST and mounted with Vectashield. Slides were stored in dark at 4°C and imaged within 1 week.

Microscopy

Slides were imaged using 100x, 1.49 NA oil immersion objective lenses on a Nikon Ti-E system fitted with a Yokogawa CSU-X1 spinning disk head (Yokogawa Corp. of America), Orca Flash 4.0 v2 digital complementary metal–oxide–semiconductor camera (Hamamatsu Corp.), Perfect

Focus system (Nikon), and a Nikon LU-N4 solid-state laser launch (15 mW; 405, 488, 561, and 647 nm). Images were acquired at ambient temperature (~25°C) using Vectashield imaging medium on Nikon Elements AR software on a 64-bit HP Z440 workstation (Hewlett-Packard). Super-resolution images were collaborated by Dr. Jordan Beach at Loyola University Chicago using a Zeiss AiryScan super-resolution microscope.

Image Analysis

Images were assembled using Fiji (National Institutes of Health; Schindelin et al., 2012) and Adobe Illustrator software to separate or merge channels, crop regions of interest, generate maximum-intensity projections, and adjust brightness and contrast.

RNA detection and measurements

A detailed protocol for RNA analysis using the Subcellular Distribution pipeline was described by Ryder and Lerit (2020). Briefly, single-channel.tif raw images were segmented using code adapted from the Allen Institute for Cell Science Cell Segmenter (Chen et al., 2018). To quantify the single-molecule RNA distribution relative to centrosomes, distances between the surface of each RNA object to the centriole zone surface of the closest centrosome were measured, and the percentage of total RNA overlapping with centrosomes was calculated. RNAs were determined to overlap with centrosomes if they were at <= 1 μm distance from the centriole surface. For *cen* mRNAs, the percentage of RNA in granules was also calculated. The Subcellular Distribution pipeline code is available on GitHub at https://github.com/pearlryder /rna-at-centrosomes and https://github.com/pearlryder/cen-at-fmr-null-centrosomes.

qPCR

RNA was extracted from ~5 mg of frozen embryos homogenized in TRI Reagent followed by phenol: chloroform extraction. To remove DNA, samples were treated with Ambion Turbo DNase (AM2238; Thermo Fisher Scientific) for 30 min at 37°C. 500 ng of RNA was synthesized into cDNA using the iScript kit according to the manufacturer's protocol (170-8891; Bio-Rad). Three biological replicates, with three technical replicates each, were loaded onto a 96-well plate (HSP9601; Bio-Rad) to perform qPCR using a Bio-Rad CFX96 real-time system with iTaq Universal SYBR Green Supermix (172–5121; Bio-Rad). *cen* and *plp* expression levels were normalized to Ribosomal protein L32 (RP49). The following primers were used: *cen* forward, 5′-TGAGGATACGACGCTCTGTG-3′, and reverse, 5′-AAAGTACCCCCGGTAACACC-3′; *plp* forward, 5'-CGCAGCAAGGAGGAGATAAC-3', and reverse, 5'-TCAGCCTGCAGTTTGTTCAC-3'; and RP49 forward, 5′-CATACAGGCCCAAGATCGTG-3′, and reverse, 5′-ACAGCTTAGCATATCGATCCG-3′.

Statistical analysis

Statistical analysis and data plotting were performed using Microsoft Excel and GraphPad Prism software. Data were first assessed with a D'Agnostino and Pearson normality test and then analyzed by Student's two-tailed *t*-test, Fisher's exact test, or nonparametric tests. Data were displayed as mean ± SD.

Chapter 2

Exploring the Regulation of *plp* mRNA Localization to Centrosomes by FMRP

As a future direction, we are interested in studying the biological importance of *plp* localization to centrosomes. Fragile-X mental retardation protein (FMRP) is an RNA-binding protein implicated in human intellectual disability. We recently showed that FMRP regulates *cen* mRNA by functionally repressing its localization to centrosomes, and excess *cen* mRNA in the absence of FMRP causes mitotic spindle defects (Ryder et al., 2020). Given this, we wanted to study whether the FMRP regulation extends to the *plp* mRNA localization to centrosomes. To examine the role of FMRP on *plp* mRNA localization, we conducted embryonic hatch rate analysis. Overnight collections of eggs were collected on yeasted grape juice agar plates, rinsed with water, and transferred to fresh plates that were marked into 20 squares with approximately 15 eggs in each square. The eggs were aged for 48 h at 25°C before counted for unhatched embryos from a total of ~300 embryos, and hatch rate was calculated from the formula, hatch rate = (total embryos – unhatched embryos) / total embryos. We found that the embryonic hatch rate of *Fmr1* null mutant (derived from $Fmr1^{\Delta 113M}/Fmr1^{3}$ trans-heterozygotes) embryos is significantly lower than WT. In contrast, the hatch rate of a rescue genotype (*Ubi-PLP/+;* $Fmr1^{\Delta 113M}/Fmr1^{3}$), expressing a PLP transgene under the Ubiquitin promotor in the *Fmr1* mutant background, is lower than the null mutant genotype (Table 1). Because the overexpression of PLP does not rescue the decreased embryonic viability in the null mutant genotype, we cannot conclude that

the absence of FMRP deregulates *plp* mRNA localization and causes lower embryonic viability. Given the decreased embryonic viability upon overexpression of PLP, we suppose that the absence of FMRP upregulates the translation of *plp* mRNA. Yet, further analysis needs to be done to study the role of FMRP on *plp* mRNA localization to centrosomes.

Replicate	Genotype	Total Embryos	Hatched Embryos	Hatch Rate	P Value
1	*yw*	837	768	92%	NA
	Fmr1 $^{\Delta 113M}$ */Fmr1* ^{3}	956	512	54%	P<0.0001 cf. WT
	Ubi-PLP/+; Fmr1 $^{\Delta 113M}$ */Fmr1* ^{3}	688	269	39%	P<0.0001 cf. WT; P<0.0001 cf. fmr1[113]/fmr1[3]
2	*yw*	837	768	92%	NA
	Fmr1 $^{\Delta 113M}$ */Fmr1* ^{3}	713	209	29%	P<0.0001 cf. WT
	Ubi-PLP/+; Fmr1 $^{\Delta 113M}$ */Fmr1* ^{3}	647	265	41%	P<0.0001 cf. WT; P<0.0001 cf. fmr1[113]/fmr1[3]
3	*yw*	837	768	92%	NA
	Fmr1 $^{\Delta 113M}$ */Fmr1* ^{3}	945	529	56%	P<0.0001 cf. WT
	Ubi-PLP/+; Fmr1 $^{\Delta 113M}$ */Fmr1* ^{3}	825	344	42%	P<0.0001 cf. WT; P<0.0001 cf. fmr1[113]/fmr1[3]

Table 1. Hatch Rate Analysis. Rescue genotype shows significantly lower embryonic viability than *Fmr1* mutants in 2 out of 3 replicates. Each replicate represents the total samples from three individual trials. P values were calculated by unpaired *t*-test.

Chapter 3

Consequences of *plp* mRNA Mislocalization at Centrosomes

Next, we studied the relationship between *plp* mRNA and PLP localization to centrosomes and the consequences of their mislocalization. To mislocalize *plp* mRNAs in *Drosophila* embryos, we designed and molecularly cloned a chimeric RNA, *pENTR-plp-bcd-3'UTR*, comprising the *plp* coding sequence and the *bicoid (bcd)-3'UTR*, which is known to be sufficient to mislocalize target RNAs to the anterior pole. While our molecular cloning strategy seemed straightforward, it proved quite difficult to simultaneously insert the large *plp* sequence and *bcd-3'UTR* into the subcloning vector. After trying three different cloning strategies and much troubleshooting (Figure 8), we have now successfully constructed the *pENTR-plp-bcd-3'UTR* construct using strategy C (Figure 8C). The breakthrough came from linearizing an existing *pENTR-plp* plasmid and subcloning in the *bcd-3'UTR* by Gibson Assembly.

To generate *pENTR-plp-bcd-3'UTR* using strategy C, the *pENTR-plp* plasmid was cut by ASC-I restriction enzyme. The *bcd-3'UTR* was PCR amplified using Phusion high fidelity DNA polymerase using primers that overlap with the restriction digest ends. The *bcd-3'UTR* was assembled and directionally cloned into the *pENTR-plp* vector by Gibson assembly using fourfold molar excess of the *bcd-3'UTR* (Figure 8C). Single colony clones were verified using Sanger sequencing. We are currently using Gateway cloning to shuttle the clone into the destination vector, *pPW-attB*, to generate transgenic animals. After obtaining our transgenic fly,

we will cross this *plp-bcd-3'UTR* transgene into the *plp* null background to eliminate endogenous *plp* expression.

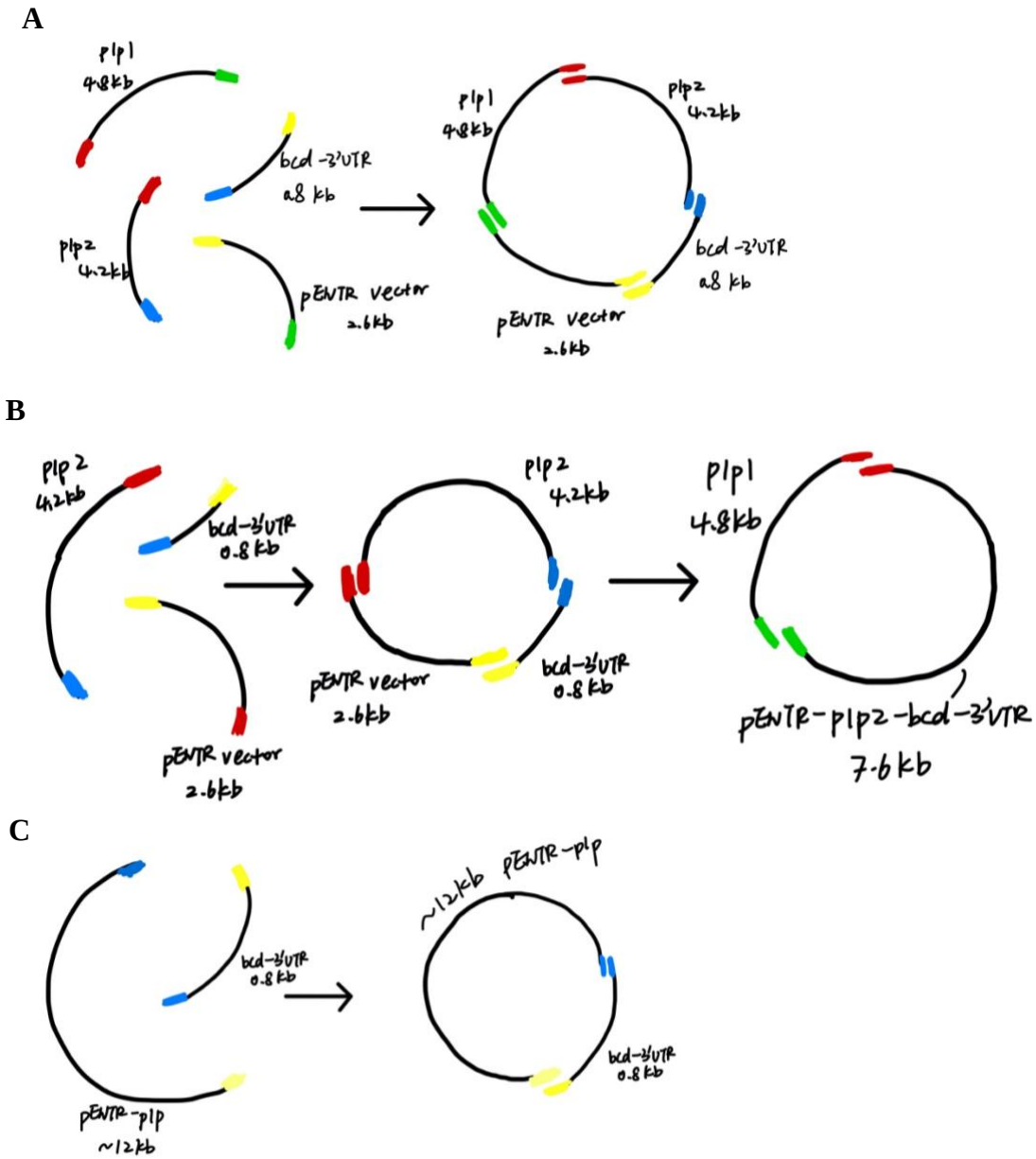

Figure 8. Molecular cloning strategies used to construct *pENTR-plp-bcd-3'UTR*. Strategy **(A)** assembles *plp* represented in two separate fragments into the subcloning vector with *bcd-3'UTR*. Strategy **(B)** suggests a two-step cloning: step 1 assembles the second fragment of *plp* and *bcd-3'UTR* into the subcloning vector to create a new vector for the second step, and step 2 assembles the first fragment of *plp* and *bcd-3'UTR* into the new vector. Strategy **(C)** assembles

bcd-3'UTR into *pENTR-plp*, which is a plasmid with full-length *plp* incorporated into *pENTR* vector.

To test whether mislocalization of *plp* mRNA prevents the normal localization of PLP protein to more distal centrosomes, we will visualize the distribution of *plp* mRNA and PLP in *plp-bcd-3'UTR* embryos using coupled smFISH and immunofluorescence (Figure 9). To study whether errant *plp* mRNA localization impair centrosome function, we will image and quantify nuclear fallout (a developmental response to DNA damage), spindle defects, and chromosome segregation using immunofluorescence. Hatch rate analysis will be also be done to investigate whether *plp* mRNA mis-localization impairs embryonic viability. Results from these experiments will confirm if localization of PLP protein to the centrosome requires localization of its transcript, *plp* mRNA, and directly address the functional relevance of a centrosome-localized mRNA.

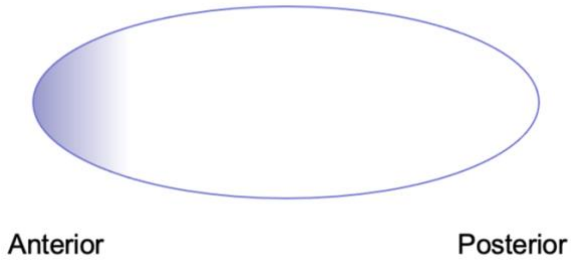

Figure 9. Expected gradient of *plp* mRNA and PLP protein mislocalized to the anterior of *plp-bcd-3'UTR* embryo. Cartoon schematic shows an early *Drosophila* embryo (ellipse) with *plp* mRNA and protein forming an anterior-directed gradient (purple shading). Because the construct is expressed in a *plp* null genetic background, no endogenous PLP is present within more distal regions.

Chapter 4

Examination of RNA Localization Relative to the Centrosome Centroid

The interphase centrosome structure is divided into three zones, i.e., centriole zone, PCM zone, and flare zone, which are 0 - 250nm, 250 - 750nm, and 1000 - 1750nm from the centroid, respectively (Figure 10). To permit the quantification of mRNA distribution at centrosomes using various centrosome markers that label various zones, we adapted our customizable Subcellular Distribution pipeline to map the mRNA distributions at the nanometer scale within the centrosome structure. To analyze mRNA distribution at centrosomes in different zones, we modified the pipeline to detect the centroid of centrosomes and quantified the mRNA distribution within a defined zone region relative to the centroid. This adaptation allows us to map mRNA localization measured from centrosome markers at different zones to the centroid of the centrosome. We wish to determine if some RNAs preferentially reside within specified sub-compartments of the centrosome and to have a more unified measurement of RNA distributions relative to any given centrosome marker. For example, we noted the apparent enrichment of cen mRNA to control centrosomes labeled with GFP-Cnn is significantly greater versus γTubulin-GFP due to the larger volume occupied by Cnn relative to γTubulin (Ryder et al., 2020).

While we initially succeeded in modifying the code (Figure 11), we noted a significant decrease in apparent *cen* mRNA localization patterns when quantified using centroid versus

surface measurements, which may be resolved by considering the single molecule normalization required to account for the large *cen* granules. We are currently testing this assumption.

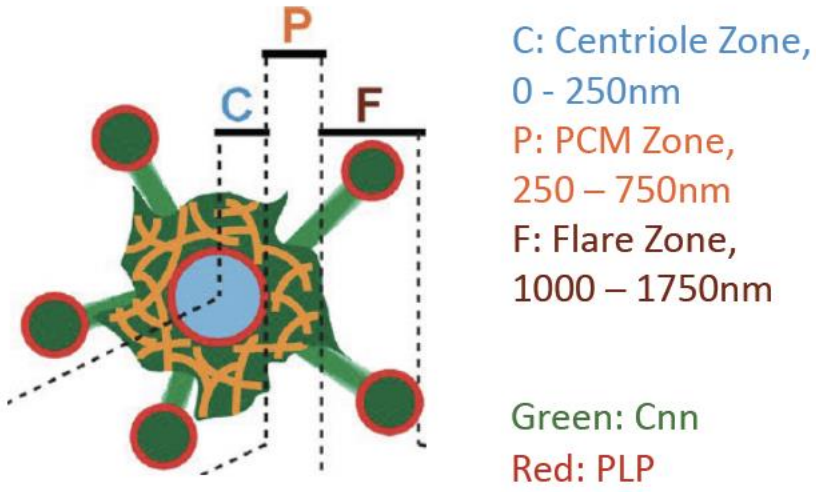

Figure 10. Structure of an interphase centrosome. (Adapted from Lerit et al., 2015) Diagram depicting an interphase specific Cnn-PLP scaffold with PLP localized to the tips of Cnn satellites in the interphase flare zone. The interphase centrosome is composed of three zones: centriole zone, PCM zone, and flare zone, which are 0 - 250nm, 250 - 750nm, and 1000 - 1750nm from the centroid, respectively.

A

```
480     # prepare the coordinates for object 1 for distance measurements
481
482     surface_coords_1 = extract_surface_coordinates(coords_1)
483     surface_coords_1 = [np.array(coord) for coord in surface_coords_1]
484
485     closest_structure_2_distance = 100000
486     closest_structure_2_id = None
487
488     # now iterate over structure 2 coords
489     for id_coord_row in structure_2_coord_data:
490         structure_2_id = id_coord_row[0]
491         coords_2 = id_coord_row[1]
492
493         surface_coords_2 = extract_surface_coordinates(coords_2)
494         surface_coords_2 = [np.array(coord) for coord in surface_coords_2]
495
496         distance_to_structure_1 = minimum_distance(surface_coords_1, surface_coords_2)
497
498         if distance_to_structure_1 < closest_structure_2_distance:
499             closest_structure_2_distance = distance_to_structure_1
500             closest_structure_2_id = structure_2_id
```

B

```
480     # prepare the coordinates for object 1 for distance measurements
481
482     surface_coords_1 = extract_surface_coordinates(coords_1)
483     surface_coords_1 = [np.array(coord) for coord in surface_coords_1]
484
485
486     closest_structure_2_distance = 100000
487     closest_structure_2_id = None
488
489     # now iterate over structure 2 coords
490     for id_centroid_row in structure_2_centroid_data:
491         structure_2_id = id_centroid_row[0]
492         centroid_2 = np.array(id_centroid_row[1])
493
494
495         distance_to_structure_1 = minimum_distance(surface_coords_1, centroid_2)
496
497         if distance_to_structure_1 < closest_structure_2_distance:
498             closest_structure_2_distance = distance_to_structure_1
499             closest_structure_2_id = structure_2_id
500
```

Figure 11. The original and modified code on the Subcellular Distribution pipeline. Modifications were made in lines 480-500 of pipeline.py on the Subcellular Distribution pipeline. **(A)** The original code calculates the distance between the surface of RNA and the surface of the centrosome marker. **(B)** Modified code that calculates the distance between the surface of RNA and the centroid of the centrosome marker. Highlighted are the changes.

References

Buxbaum, A.R., G. Haimovich, and R.H. Singer. 2015. In the right place at the right time: visualizing and understanding mRNA localization. *Nat Rev Mol Cell Biol*. 16:95-109.

Chouaib, R., A. Safieddine, X. Pichon, A. Imbert, O.S. Kwon, A. Samacoits, A.-M. Traboulsi, M.-C. Robert, N. Tsanov, E. Coleno, I. Poser, C. Zimmer, A. Hyman, H. Le Hir, K. Zibara, M. Peter, F. Mueller, T. Walter, and E. Bertrand. 2020. A Dual Protein-mRNA Localization Screen Reveals Compartmentalized Translation and Widespread Co-translational RNA Targeting. *Developmental cell*. 54:773-791.e775.

Conduit, P.T., A. Wainman, and J.W. Raff. 2015. Centrosome function and assembly in animal cells. *Nat Rev Mol Cell Biol*. 16:611-624.

Dalby, B., and D.M. Glover. 1992. 3′ non-translated sequences in Drosophila cyclin B transcripts direct posterior pole accumulation late in oogenesis and peri-nuclear association in syncytial embryos. *Development*. 115:989-997.

Fang, J., and D.A. Lerit. 2022. Orb-dependent polyadenylation contributes to PLP expression and centrosome scaffold assembly. *Development*. 149.

Femino, A.M., F.S. Fay, K. Fogarty, and R.H. Singer. 1998. Visualization of single RNA transcripts in situ. *Science*. 280:585-590.

Foe, V.E., and B.M. Alberts. 1983. Studies of nuclear and cytoplasmic behaviour during the five mitotic cycles that precede gastrulation in Drosophila embryogenesis. *J Cell Sci*. 61:31-70.

Kao, L.R., and T.L. Megraw. 2009. Centrocortin cooperates with centrosomin to organize Drosophila embryonic cleavage furrows. *Curr Biol*. 19:937-942.

Khodjakov, A., and C.L. Rieder. 1999. The sudden recruitment of gamma-tubulin to the centrosome at the onset of mitosis and its dynamic exchange throughout the cell cycle, do not require microtubules. *J Cell Biol*. 146:585-596.

Lécuyer, E., H. Yoshida, N. Parthasarathy, C. Alm, T. Babak, T. Cerovina, T.R. Hughes, P. Tomancak, and H.M. Krause. 2007. Global analysis of mRNA localization reveals a prominent role in organizing cellular architecture and function. *Cell*. 131:174-187.

Lerit, D.A., H.A. Jordan, J.S. Poulton, C.J. Fagerstrom, B.J. Galletta, M. Peifer, and N.M. Rusan. 2015. Interphase centrosome organization by the PLP-Cnn scaffold is required for centrosome function. *Journal of Cell Biology*. 210:79-97.

Lerit, D.A., H.A. Jordan, J.S. Poulton, C.J. Fagerstrom, B.J. Galletta, M. Peifer, and N.M. Rusan. 2015. Interphase centrosome organization by the PLP-Cnn scaffold is required for centrosome function. *The Journal of cell biology*. 210:79-97.

Lerit, D.A., H.A. Jordan, J.S. Poulton, C.J. Fagerstrom, B.J. Galletta, M. Peifer, and N.M. Rusan. 2015. Interphase centrosome organization by the PLP-Cnn scaffold is required for centrosome function. *J Cell Biol*. 210:79-97.

Lerit, D.A., and N.M. Rusan. 2013. PLP inhibits the activity of interphase centrosomes to ensure their proper segregation in stem cells. *Journal of Cell Biology*. 202:1013-1022.

Magescas, J., J.C. Zonka, and J.L. Feldman. 2019. A two-step mechanism for the inactivation of microtubule organizing center function at the centrosome. *Elife*. 8.

Martinez-Campos, M., R. Basto, J. Baker, M. Kernan, and J.W. Raff. 2004. The Drosophila pericentrin-like protein is essential for cilia/flagella function, but appears to be dispensable for mitosis. *J Cell Biol*. 165:673-683.

Mittasch, M., V.M. Tran, M.U. Rios, A.W. Fritsch, S.J. Enos, B. Ferreira Gomes, A. Bond, M. Kreysing, and J.B. Woodruff. 2020. Regulated changes in material properties underlie centrosome disassembly during mitotic exit. *J Cell Biol*. 219.

Nigg, E.A., and J.W. Raff. 2009. Centrioles, centrosomes, and cilia in health and disease. *Cell*. 139:663-678.

Palazzo, R.E., J.M. Vogel, B.J. Schnackenberg, D.R. Hull, and X. Wu. 2000. Centrosome maturation. *Curr Top Dev Biol*. 49:449-470.

Raff, J.W., W.G. Whitfield, and D.M. Glover. 1990. Two distinct mechanisms localise cyclin B transcripts in syncytial Drosophila embryos. *Development*. 110:1249-1261.

Rauch, A., C.T. Thiel, D. Schindler, U. Wick, Y.J. Crow, A.B. Ekici, A.J. van Essen, T.O. Goecke, L. Al-Gazali, K.H. Chrzanowska, C. Zweier, H.G. Brunner, K. Becker, C.J. Curry, B. Dallapiccola, K. Devriendt, A. Dörfler, E. Kinning, A. Megarbane, P. Meinecke, R.K. Semple, S. Spranger, A. Toutain, R.C. Trembath, E. Voss, L. Wilson, R. Hennekam, F. de Zegher, H.G. Dörr, and A. Reis. 2008. Mutations in the pericentrin (PCNT) gene cause primordial dwarfism. *Science*. 319:816-819.

Ryder, P.V., J. Fang, and D.A. Lerit. 2020. centrocortin RNA localization to centrosomes is regulated by FMRP and facilitates error-free mitosis. *J Cell Biol*. 219.

Ryder, P.V., and D.A. Lerit. 2020. Quantitative analysis of subcellular distributions with an open-source, object-based tool. *Biology Open*. 9.

Safieddine, A., E. Coleno, S. Salloum, A. Imbert, A.-M. Traboulsi, O.S. Kwon, F. Lionneton, V. Georget, M.-C. Robert, T. Gostan, C.-H. Lecellier, R. Chouaib, X. Pichon, H. Le Hir, K. Zibara, F. Mueller, T. Walter, M. Peter, and E. Bertrand. 2021. A choreography of

centrosomal mRNAs reveals a conserved localization mechanism involving active polysome transport. *Nature Communications*. 12:1352.

Sepulveda, G., M. Antkowiak, I. Brust-Mascher, K. Mahe, T. Ou, N.M. Castro, L.N. Christensen, L. Cheung, X. Jiang, D. Yoon, B. Huang, and L.E. Jao. 2018. Co-translational protein targeting facilitates centrosomal recruitment of PCNT during centrosome maturation in vertebrates. *Elife*. 7.

Sorokin , S. 1962. CENTRIOLES AND THE FORMATION OF RUDIMENTARY CILIA BY FIBROBLASTS AND SMOOTH MUSCLE CELLS. *Journal of Cell Biology*. 15:363-377.

Vastenhouw, N.L., W.X. Cao, and H.D. Lipshitz. 2019. The maternal-to-zygotic transition revisited. *Development*. 146.